Polyaniline-graphene based α-amylase biosensor with a linear dynamic range in excess of 6 orders of magnitude

Sofia Teixeira, Catherine Lloyd, Seydou Yao, Andrea Gazze, Iain S Whitaker, Lewis Francis, R. Steven Conlan, Ernest Azzopardi

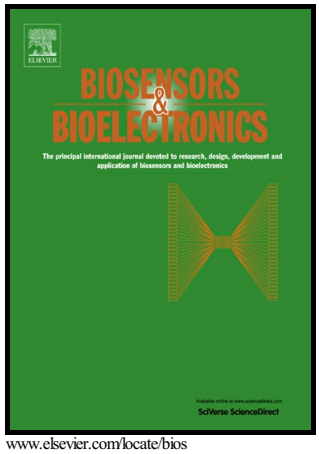

www.elsevier.com/locate/bios

PII: S0956-5663(16)30458-4
DOI: http://dx.doi.org/10.1016/j.bios.2016.05.034
Reference: BIOS8724

To appear in: *Biosensors and Bioelectronic*

Received date: 2 February 2016
Revised date: 21 April 2016
Accepted date: 8 May 2016

Cite this article as: Sofia Teixeira, Catherine Lloyd, Seydou Yao, Andrea Gazze, Iain S Whitaker, Lewis Francis, R. Steven Conlan and Ernest Azzopardi Polyaniline-graphene based α-amylase biosensor with a linear dynamic range i excess of 6 orders of magnitude, *Biosensors and Bioelectronic* http://dx.doi.org/10.1016/j.bios.2016.05.034

Polyaniline-graphene based α-amylase biosensor with a linear dynamic range in excess of 6 orders of magnitude.

Sofia Teixeira[1,3*], Catherine Lloyd[1,2,3], Seydou Yao[2,3], Andrea Gazze[2,3], Iain S Whitaker[2,4], Lewis Francis[2,3], R. Steven Conlan[2,3], Ernest Azzopardi[2,4]

[1]College of Engineering, Swansea University, Bay Campus, Swansea, SA1 8QQ, UK

[2]Swansea University Medical School, Singleton Park, Swansea, SA2 8PP, UK

[3]Centre for NanoHealth, Swansea University, Singleton Park, Swansea, SA2 8PP, UK

[4]The Welsh Centre for Burns and Plastic Surgery, Morriston Hospital, Swansea, SA66NL, UK

[*]Correspondence address: College of Engineering, Swansea University, Fabian Way, Skewen, SA1 8EN, Swansea, UK. Tel: +44 01792606182. E-mail address: r.rodriguesteixeira@swansea.ac.uk

Abstract

α-amylase is an established marker for diagnosis of pancreatic and salivary disease, and recent research has seen a substantial expansion of its use in therapeutic and diagnostic applications for infection, cancer and wound healing. The lack of bedside monitoring devices for α-amylase detection has hitherto restricted the clinical progress of such applications.

We have developed a highly sensitive α-amylase immunosensor platform, produced via *in situ* electropolymerization of aniline onto a screen-printed graphene support (SPE). Covalently binding an α-amylase specific antibody to a polyaniline (PANI) layer and controlling device assembly using electrochemical impedance spectroscopy (EIS), we have achieved a highly linear response against α-amylase concentration. Each stage of the assembly was characterized using a suite of high-resolution topographical, chemical and mechanical techniques. Quantitative, highly sensitive detection was demonstrated using an artificially spiked human blood plasma samples. The device has a remarkably wide limit of quantification (0.025-1000 IU/L) compared to α-amylase assays in current clinical use. With potential for simple scale up to volume manufacturing though standard semiconductor production techniques and subsequently clinical application, this biosensor will enable clinical benefit through early disease detection, and better informed administration of correct therapeutic dose of drugs used to treat α-amylase related diseases.

Keywords: Immunosensor; Screen-printed electrode; Graphene; Antibody; Polyaniline; α-amylase.

1. Introduction

α-amylase was the very first enzyme to be discovered and characterized (Whitcomb and Lowe 2007) and has been used for the past two centuries as a disease biomarker. α-amylase is a well-established marker for the diagnosis, monitoring of progression and outcome of pancreatic disease, a common cause of hospital admissions with high morbidity and mortality (Seetharaman and Bertoft

2012). Despite this historic utility, it is only very recently that a substantial expansion of its role into therapeutic and diagnostic applications in other areas of high clinical demand including inflammation, infection, cancer and wound healing has occurred (Azzopardi et al. 2013, 2014, 2015; Duncan 2014). In particular, amylase has been extensively investigated as a trigger for controlled, bioresponsive release of advanced therapeutics such as dextrin conjugates of growth factors, antibiotics, and anticancer agents (Duncan 2008; Hardwicke et al. 2008). It is also exploited as a replacement enzyme, whilst some of its inhibitors are clinically licenced for the treatment of diabetes and weight management.

Current α-amylase assays in clinical use are laboratory based, utilize analytical equipment with a large footprint, have an appreciable turnaround time (TAT), measure activity rather than concentration, and are susceptible to hemolysis and inactivation. These substantial limitations restrict further expansion of α-amylase based diagnostics and theranostics into viable clinical practice. Moreover, the host of controlled release medications that have been developed on the premise of α-amylase activated release would benefit from rapid, accurate, point-of-care quantification (Hardwicke et al. 2008; Gaspar and Duncan 2011; Azzopardi et al. 2014, 2015). Furthermore, availability of bedside diagnostics would push the scope of these applications from secondary into primary care, leading to improved clinical and economic outcomes (Price 2001).

Due to their ease of manufacture, high-sensitivity and potential for miniaturization, electrochemical immunosensors have emerged as a major technology platform for point of care /at the bedside (POC/B) biomarker detection (Tothill 2009). Electrochemical impedance spectroscopy (EIS) enables detection and signal output due to its ability to measure subtle changes in the electrochemical properties of materials at their interface with conducting electrodes (Ensafi and Karimi-Maleh 2010; Beitollah et al., 2012; Shahmiri et al., 2013; Moradi et al., 2013; Karimi-Maleh et al., 2013; Karimi-Maleh et al., 2014). Gold, zinc oxide, iron oxide, and carbon are the main substrates that are being developed for use in such sensors (Pena Pereira et al. 2012). Carbon nanostructures, and more

recently graphene, are now being widely adopted as alternatives to gold as electrode substrates (Pumera et al., 2010; Song and Xuefeng 2012; Wenjing et al., 2013; Toktam et al., 2014). Graphene is of particular interest as a biosensor platform due to intrinsic properties such as its large surface area, high electrical conductivity and biocompatibility (Dan et al., 2008; Jing et al., 2009; Li et al., 2009; Qin et al., 2011). Graphene based devices have been developed that can measure minute changes in analyte concentration levels, and have been used to detect for cancer tumor markers, human chorionic gonadotrophin (hCG) and markers of cardiac diseases (Yasufumi et al., 2010; Hyun Jung et al., 2010; Nguyen Xuan et al., 2013; Zhang et al., 2015).

Composed of sp^2 carbon, graphene is chemically unsaturated. Intrinsically, it can undergo covalent addition to change the carbons from sp^2 to sp^3 following hybridization, however, carbon atoms in the graphene basal plane are protected by their π-conjugation system, the motion of which is constrained by surrounding carbon atoms. Therefore, basal plane covalent addition usually encounters large energy barriers, and reactive chemical groups, such as atomic hydrogen, fluorine, and pre-cursors of other chemical radicals, are usually needed as reactants. The controlled functional association of biomolecules with graphene is therefore key to developing any high throughput biosensor platform. The chemical modification of graphene is difficult to control, with reactions occurring predominantly at the surface edge thereby limiting surface reactivity and limits of detection (Martin 2011). Additionally, defects can be introduced to the graphene through functionalization procedures, which are required to immobilize biomolecules to the graphene surface.

Polyaniline (PANI) is a conductive polymer and has been widely used as an additive transducer layer in sensors to avoid the introduction of graphene surface defects (Ates 2013). In addition the use of PANI improves antibody attachment to sensor electrodes while preserving optimal electrical characteristics (Wang et al., 2011; Ates 2013). In addition, PANI has excellent acid/base sensitivity, a huge range of tunable conductivity, (Srinives et al., 2015) redox sensitivity, environmental stability, (Ruecha et al., 2015; Zhang et al., 2015) short reversible response times, (Nipapan Ruecha

2015) and is easily synthesized (Nipapan Ruecha 2015) and functionalized. A detailed description of state of the art sensors under development or fully developed is provided in the supplementary material.

The present work describes an approach toward the development of an α-amylase specific immunosensor, using a combination of electro-polymerization of PANI on a graphene support and subsequent antibody binding to the polymer film. The biosensor platform enables fully quantitative analysis of analyte concentrations in a simulated biological sample and in human plasma. The device displays a linear response to increasing α-amylase concentration between 1 and 1000 International Units/L (IU/L), and a LOD of 0.025 U/L.

2. Experimental Section

2.1. Chemicals and Materials

All chemicals used were of analytical grade and water was ultrapure grade. Potassium hexacyanoferrate III ($K_3[Fe(CN)_6]$), potassium hexacyanoferrate II ($K_4[Fe(CN)_6]$) trihydrate, *N*-(3-Dimethylaminopropyl)-*N'*-ethylcarbodiimide hydrochloride (EDAC), *N*-Hydroxysuccinimide (NHS), bovine serum albumin (BSA), Phosphate Buffered Saline (PBS) and aniline were obtained from Sigma Aldrich-UK; alpha-amylase and anti-α-amylase antibody was purchased from Abcam (UK); A 0.1 M aniline solution was prepared in 2.5 M H_2SO_4. EDAC, NHS and antibody solutions were prepared in PBS buffer. A redox probe solution was prepared in PBS buffer to a concentration of 5.0 mmol/L of $[Fe(CN)_6]^{3-}$ and 5.0mmol/L of $[Fe(CN)_6]^{4-}$

2.2. Apparatus

Electrochemical measurements were conducted with a potentiostat/galvanostat, Metrohm Autolab, PGSTAT302N, controlled by Nova software and equipped with a Frequency Response Analysis module. Graphene-SPEs were purchased from DropSens (DRP-110GPH) and were composed of a

carbon counter electrode, an silver pseudo-reference electrode, and a printed graphene working electrode (4 mm ∅). Electrical characterization of SPEs was performed by connecting the SPEs to the potentiostat/galvanostat *via* a suitable switch box (DropSens).

Micro-Raman measurements were performed using a Renishaw InVia system with a 100 mW 532 nm excitation laser with approximately 10 mW of power on the sample. Ultra-high resolution SEM measurements were performed using a Hitachi High-Technologies S-4800 and AFM measurements were performed using a BioScope Catalyst™ BioAFM.

Atomic Force Microscopy (AFM) samples were imaged in PeakForce Tapping using a Bruker BioScope Catalyst. NanoWorld Arrow^{TM} NCR cantilevers, with a nominal spring constant of 42 N/m, were used as probes. A total of three regions per sample were imaged, each region having an area of 25 μm^2. The roughness subroutine in the Nanoscope Analysis software, v1.50, was used. For each 25 μm^2 region the RMS roughness R_q (Equation1) was measured on ten different areas of 1 μm^2 each, according to the procedure described in (Lewis et al., 2009):

$$R_q = \sqrt{\frac{\sum Z_i^2}{N}} \qquad (1)$$

where, N is the number of height points in the analyzed area and Z_i is the vertical distance of data point i from the mean image data plane.

2.3. Single Molecule Force Spectroscopy

All experiments were performed using a JPK Nanowizard II AFM (JPK, Berlin, Germany). A two-step chemical procedure was developed in order to link the amylase protein to the AFM probe surface. Briefly, after a 5-min wash in acetone, triangular silicon nitride cantilevers (DNP-10; Bruker-nano, Coventry, UK) were cleaned by immersion in piranha solution (H_2SO_4:H_2O_2; 3:1; v/v) for 30 min. The cantilevers were then incubated with 1ml of 0.1% w/v of APTES pH 7.2 for 10 min, creating an amino-terminated tip surface, which were rinsed several times with PBS and water before

incubation with LC-SPDP for 45 min to obtain a reactive pyridyl-disulfide surface. The amylase protein (Abcam, concentration : 300ug/ml) was modified by reaction with SATP for 30min in order to produce a free sulfhydryl group, followed by a series of purification steps through a dextran column (Fischer scientific). LC-SPDP functionalized cantilevers were then washed and incubated in the presence of thiolated activated amylase, forming an Amylase functionalised probe through a disulfide exchange reaction with SPDP-activated protein (thiol chemistry is less sensitive to hydrolysis in aqueous solution compared to NHS chemistry, and thus enables the use of longer incubation times for efficient conjugation(Chemical Functionalization and Bioconjugation Strategies for Atomic Force Microscope Cantilevers (Magnus Bergkvist 2011).

Set to operate in force spectroscopy mode, amylase functionalised DNP-10 (Bruker Nano, Coventry, UK) probes were used, with nominal spring constants of 0.065N/m following functionalization (checked using the Thermal tune method). The maximum load force was set at 1.5nN and the z speed for both extend and retract adjusted to 4um/s. A force delay of 200ms was added to ensure contact time between the Amylase protein and the substrate surface. Data was collected from all channels and 768 force curves were collected as a series of 16x16 FV maps, from negative control, non-activated amylase and F_c region activated Amylase substrates to monitor alterations in the adhesions affinity of the device surface. A minimum of 3 biological repeats were used for this study and all data shown is representative of the binding rupture arrays observed.

2.4. Surface modification

The polyaniline (PANI) film was obtained according to our previous work (Teixeira at al., 2014). A drop of activated antibody solution was added to the PANI layer on the working electrode, and incubated for 2 hours, at room temperature. The activated antibody solution had been pre-prepared, by incubating a 0.5 mg/mL antibody solution in 25 mmol/L EDAC and 50 mmol/L of NHS, for 2 hours, at room temperature. Following exposure of the working electrode to the activated antibody solution the working electrode was then rinsed with PBS and incubated in BSA solution (0.5 mg/mL

in PBS), for 30 minutes. The immunosensor was then washed (3 times) with PBS and kept at 4ºC until use.

2.5. Alpha-amylase binding

Alpha-amylase binding to the immobilized antibody was achieved by placing a drop of alpha-amylase solution on the immunosensor working electrode surface. Different concentrations of alpha-amylase solutions, ranging from 0.01 to 1000 U/L, were prepared by dilution of the 1000 U/mL standard alpha-amylase solutions in PBS or plasma. Alpha-amylase was also detected in human plasma samples and pus samples from patients. A period of 15 minutes was allowed for antigen/antibody binding. This was followed by PBS washing (3 times) prior to redox probe EIS measurements.

2.6. Electrochemical measurements

CV and EIS assays were conducted in triplicate. CV measurements were conducted in 5.0 mmol/L of $[Fe(CN)_6]^{3-}$ and 5.0 mmol/L of $[Fe(CN)_6]^{4-}$, prepared in PBS buffer, pH 7.4, using a potential scan from -0.7 to +0.7 V, at 50 mV/s. EIS assays were made using the same redox couple $[Fe(CN)6]^{3-/4-}$ solution, at a standard potential of +0.10 V, using a sinusoidal potential perturbation with amplitude of 100 mV and a frequency of 50 Hz, logarithmically distributed over a frequency range of 1000-0.01 Hz. Impedance data was fitted to a [R(C[R(RC)])] circuit, using the Nova Software.

The immunosensor response to varying alpha-amylase concentrations was assessed by EIS measurements. The Limit of Detection (LOD) was defined as the alpha-amylase concentration at which the calibration curve corresponded to a signal of 3σ, where σ is the standard deviation of EIS blank signals (obtained in the absence of the alpha-amylase).

3. Results and discussion

3.1. Coating of screen-printed graphene electrode with thin film polyaniline

A screen-printed graphene electrode was functionalized *via* polymerization with a thin film of polyaniline to provide amine groups on the SPE-graphene/ PANI (Figure 1B). The PANI film was formed by coating the electrode in a solution of aniline and subsequent electropolymerization to form a conductive polymer layer over the graphene support, enabling the transport of electron carriers to the graphene SPE (Li et al., 2009; Bhadra et al., 2011; Zhixiang et al., 2012; Zi-Long et al., 2012).

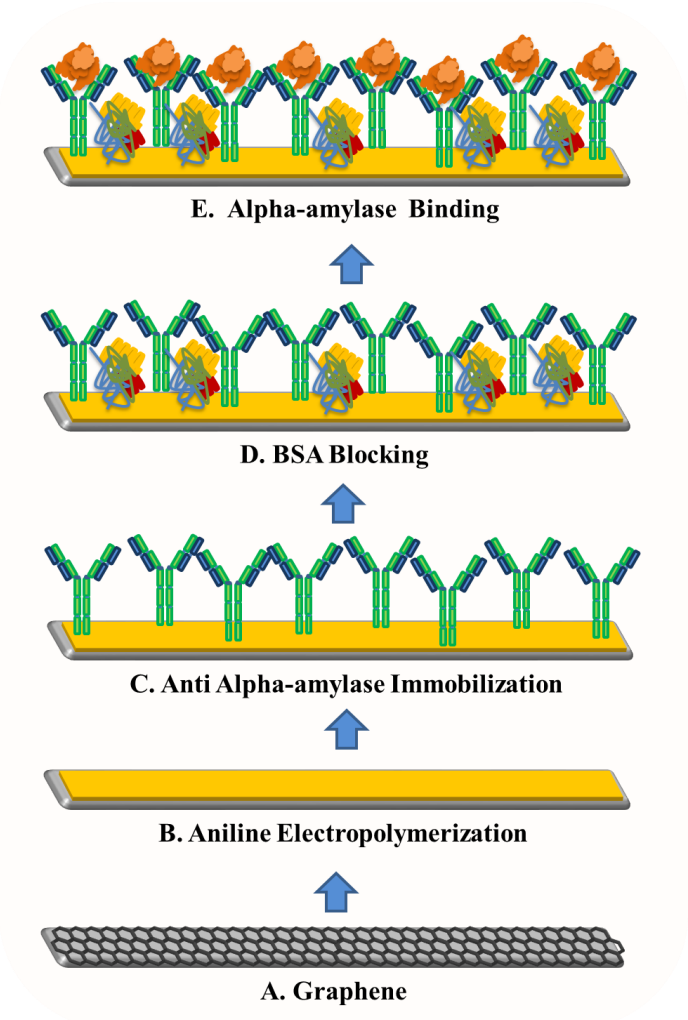

Figure 1. Schematic diagram for the immunosensor assembly.

Having deposited polyaniline, the sensor was then functionalized through covalently linking a α-amylase antibody to the PANI layer (Figure 1C). A carbodiimide crosslinker chemistry EDAC/NHS

was used for the specific activation of the –COOH terminated amino acid chains in the antibody. This forms a highly reactive *O*-Acylisourea intermediate that rapidly reacts with NHS to produce a stable succinimydyl ester (Kuiyang et al., 2004). This ester then undergoes a nucleophilic substitution reaction with the amine groups on the PANI, leading to the formation of an orientated antibody grafted PANI layer (Figure 1C). Due to exposure to the EDAC/NHS reagents, it is possible that each of -COOH groups at the antibody may have been activated. It is not possible therefore to ensure exclusive antibody binding through the F_c region, only that orientation via the F_c region is significantly higher than with random antibody adsorption. Bovine serum albumin (BSA) was then added to the sensor surface randomly (Figure 1D), and serves to prevent any non-specific interactions with the sensor surface thereby eliminating the possibility of the sensor generating any non-specific background signal.

3.2. Single Molecule Force Spectroscopy

In order to demonstrate the stability of antigen–antibody binding during the device development process single molecule force spectroscopy (SMFS), using an amylase-functionalized silicon nitride cantilever was employed (Yi Cao et al., 2007; Fuhrmann and Ros 2010; Chunmei Lv et al., 2014). A short LC-SPDP (sulfosuccinimidyl 6-(3'-(2-pyridyldithio)propionamido)hexanoate) linker molecule was used to permit free rotation of the immobilized amylase protein on the probe, mimicking amylase mobility at the substrate surface in solution (Ebner 2007; Neundlinger et al., 2011). Following dynamic ramping of the α- amylase probes to the sensor surface, the force distance curve data was used to determine the stability of the covalent cross linking at the PANI antibody interface and its effect on sensor affinity for its target analyte. Figure 2, shows that both the ‘random adsorption (non-activated Ab)’ and ‘EDAC/NHS linker (F_c activated Ab coupling)’ substrate surfaces resulted in a high number of specific force rupture events in the AFM retraction curve (47%

and 53% of total curves respectively) demonstrating retention of antibody function on the PANI-graphene surface.

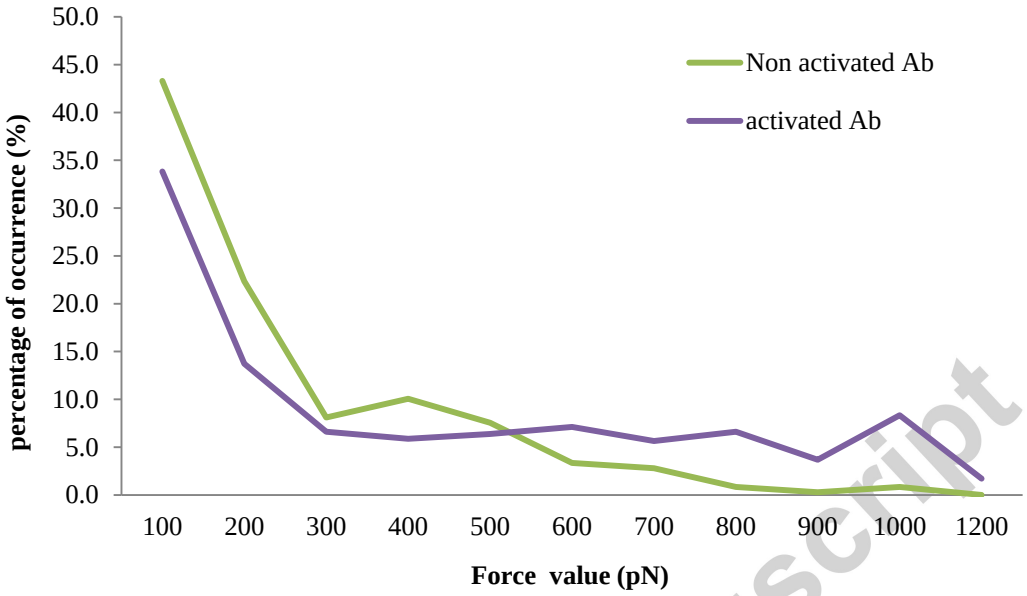

Figure 2. Percentage of occurrence of steps according to their force values for the activated antibody (Ab) compare to the non-activated antibody.

A significantly higher percentage (40 %) of rupture events occurred at a force above 500pN with the 'EDAC/NHS linker (F_c activated Ab coupling)' sample compared to just 16% for the random adsorption (non-activated samples) (Figure 2). This indicates that EDAC/NHS coupling achieves an increased percentage of F_c immobilized antibodies compared to the random adsorption method.

3.3. Qualitative analysis of the immunosensor surface

Throughout the sensor development process a series of surface characterization techniques were used to monitor the step-wise assembly of the device to inform process optimization.

Raman Spectroscopy (RS) - Raman spectra indicate the chemical nature of the surface through molecular vibrational transitions. RS was used here to provide information on the structure, carbon atom hybridization state, defects, functionalization and graphene layer depth during the fabrication

stages (Figure 3) (Nafie 2001). Control graphene-SPE spectra showed three Raman bands at 1350, 1600 and 2700 cm^{-1} that are assigned to the well-documented D, G and 2D bands in standard graphene (Elias et al., 2009). The G band represents the in-plane bond-stretching vibrations of sp^2-hybridized carbon atoms, while band D is related to the vibrations of the carbon atoms of sp^3-hybridised carbon atoms of disordered and/or defected graphite (Elias et al., 2009). The intensity ratio of I_G/I_D bands can be used to quantify the defect density in graphene. The I_G/I_D ratio measured on the sensor surface for graphene was 1.15 and 1.18 respectively (Figure 3A and B) indicating significant disorder as a result of structural defects (Jijun Ding 2013).

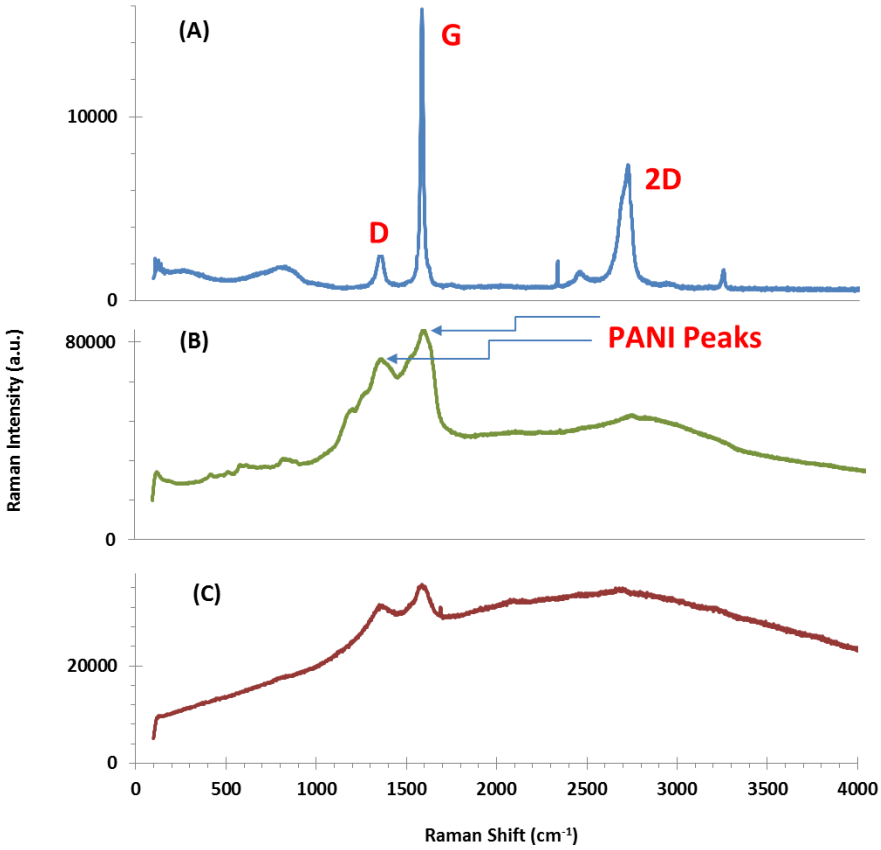

Figure 3. Raman spectra of (A) graphene-SPE, (B) PANI/graphene-SPE and (C) anti-alpha amylase/PANI/graphene-SPE.

Similar spectra were obtained from both SPE-Graphene/PANI (Figure 3B) and SPE-Graphene/PANI/Ab (Figure 3C) surfaces, showing an increased intensity of D peak, corresponding to an I_G/I_D ratio equal to 1.16 when compared to the control. After electrochemical polymerization, all of the Raman spectra exhibited distinct bands attributable to PANI, (Da-Wei et al, 2009) which overlap the characteristic bands of standard graphene (at 1300 and 1600 cm^{-1}; Figure 3 B). The sp^3 graphene peak became more intense and broad following PANI deposition, (Yan Liu 2012) resulting in a significant increase in the intensity ratio of bands D/G. Antibody binding therefore introduced an additional increase in the Raman intensity (Figure 3C).

3.4. Scanning Electron (SEM) and Atomic Force Microscopy (AFM)

The morphology, topography and structure of the SPE-graphene following each fabrication stage were also characterized using both SEM and AFM (Figure 4).

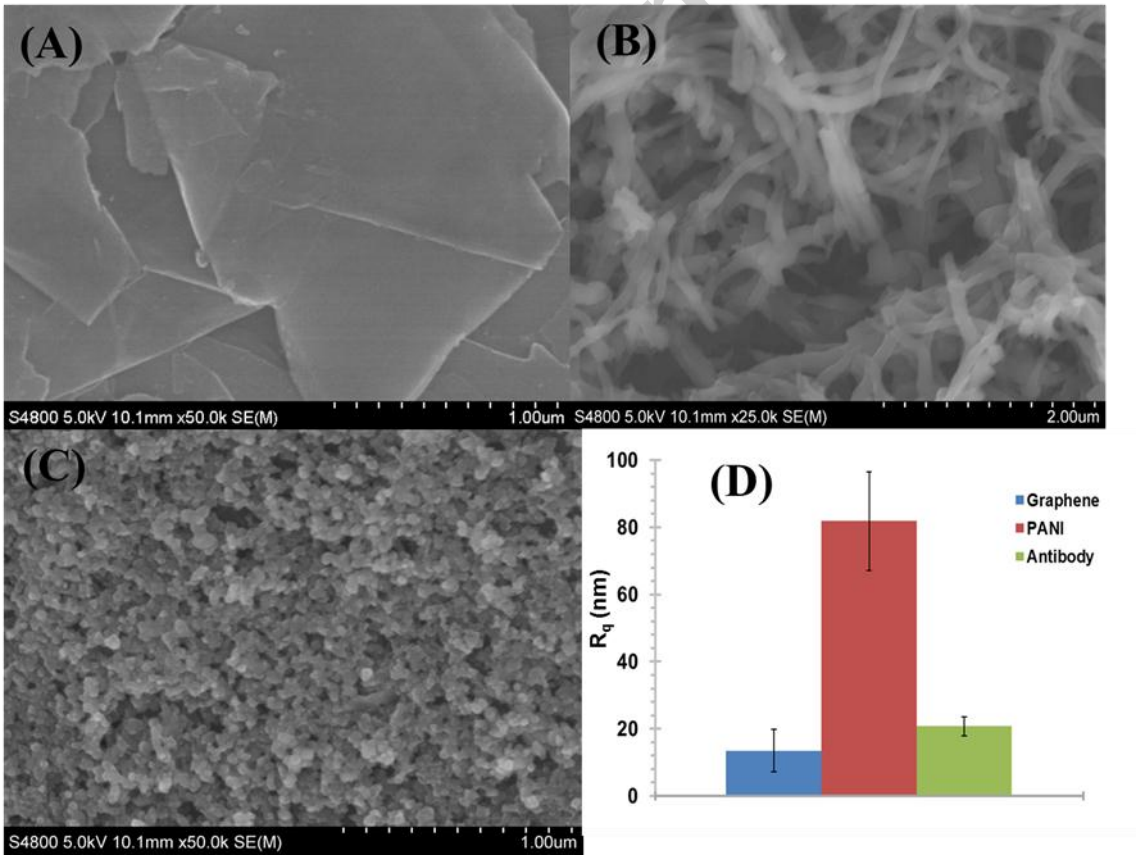

Figure 4. SEM images of: (A) unmodified graphene; (B) graphene modified with PANI (C); Antibody attached to the PANI layer and (D) Plot of the roughness R_q for the different samples: Graphene R_q= 13.5 ± 6.36 nm; PANI R_q=81.9 ± 14.8 nm; Antibody R_q= 20.8 ± 2.86 nm.

Unmodified graphene exhibits a flat, smooth area with few significant topographical features (Figure 4A). The addition of PANI results in the introduction of a fibrous structure following the electropolymerization process was observed at both the micro and nanoscale (Figures 4B) which demonstrates that the polymer is in a crystalline form (Kavitha et al., 2012). Following the functionalization with the anti- α-amylase antibody, the fibrous structure becomes uniformly coated with globular antibody clusters (Figures 4C).

Surface roughness (Rq) analysis using AFM further demonstrated the reproducibility of each stage of the fabrication process. (Figure 4D). Non-functionalized graphene exhibited lower Rq values of 13.5 ± 6.36 nm. The addition of PANI resulted in a significant increased Rq of 81.9 ± 14.8 nm ($P<0.001$), and following antibody addition, the surface Rq values significantly decreased to 20.8 ± 2.86 nm ($p<0.001$).

3.5. Electrochemical characterization

The effects of modifications at the graphene surface were monitored using cyclic voltammetry (CV) and electrochemical impedance spectroscopy (EIS) respectively, in order to characterise changes in electron transfer properties against the redox probe (Jonathan and Nader 2007). Nyquist plots were used to show the frequency response of the electrode/electrolyte system and an area plot of the imaginary component (Z``) of the impedance against the real component (Z`) (Figure 5). The charge-transfer resistance (Rct) at the electrode surface is depicted by a semi-circular output plot obtained from EIS that can be used to define the interface properties of the electrode.

As shown in Figure 5A a peak-to-peak potential difference (ΔEp) and peak-to-peak current difference (ΔIp) of the $[Fe(CN)6]^{3-/4-}$ redox couple show the changes at each step of the surface modification of graphene-SPE. The unmodified graphene-SPE shows a quasi-reversible electrochemical response for the $[Fe(CN)6]^{3-/4-}$ redox couple with ΔEp of 0.164 V and ΔIp of 0.248 mA. The modification of graphene-SPE surface with PANI in a ΔIp increase of 0.139 mA and a ΔEp decrease of 0.241 V. This result is attributed that a positively charged amino group of the PANI molecule which attracts the negative charge of $[Fe(CN)6]^{3-/4-}$, causing an easy electron transfer reaction on the electrode surface (Erhan et al., 2013).

A cyclic voltammogram of the SPE-graphene/PANI/Ab electrode showed a decrease peak-to-peak potential separation (ΔEp of 0.088 V). Further, addition of the BSA blocking agent to the SPE-graphene/PANI/Ab electrode surface gave rise to a change on the electrochemical behavior of the $[Fe(CN)6]^{3-/4-}$ couple, leading to ΔEp increase of 0.03 V and decreased ΔIp value of 0.067 mA. BSA molecules cause masking of the electrode surface for oxidation/reduction of the redox probe $[Fe(CN)6]^{3-/4-}$ (Heli et al., 2007).

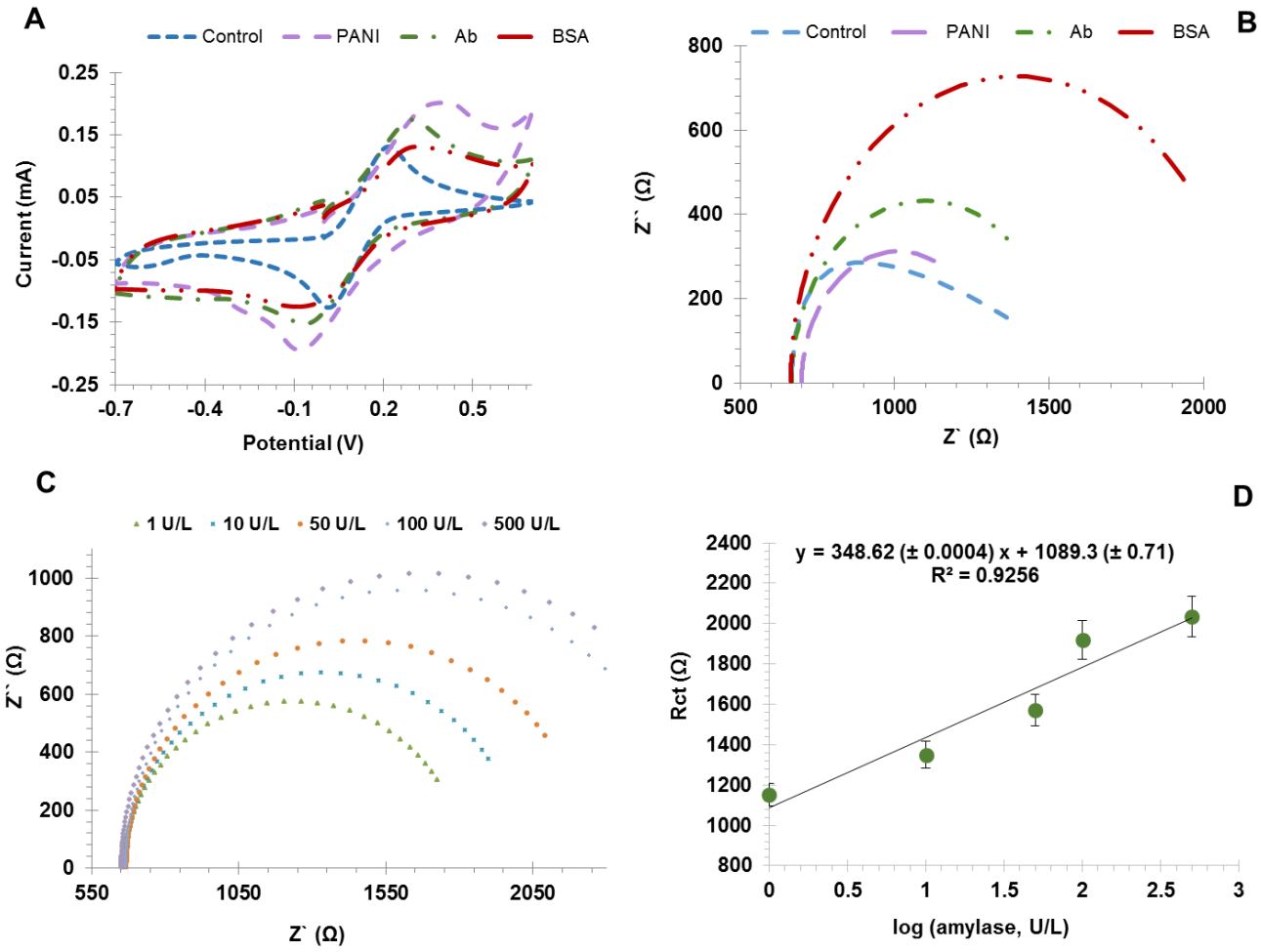

Figure 5. CV data taken at each assembly stage of the immunosensor (A), EIS spectra of each stage (B). (A) CV record after modification of PANI/graphene-SPE with antibody and BSA. (B) Nyquist plots of BSA/anti-alpha amylase/PANI/graphene-SPE sensor, obtained in 5.0mM $[Fe(CN)6]^{3-/4-}$ PBS buffer pH 7.4. EIS spectra of calibration along with its calibration plot (C) and (D). (C) Nyquist plots of the BSA/anti-alpha amylase/PANI/graphene-SPE sensor, previously incubated in increasing concentrations of amylase, obtained in obtained in 5.0mM $[Fe(CN)6]^{3-/4-}$ PBS buffer pH 7.4; (D) the Rct values of the previous calibration plotted against log amylase concentration, with a standard deviation of 13.929%.

The unmodified graphene surface shows a very fast electron-transfer process (Rct = 572.5 Ω, Figure 5B). Following the electrochemical deposition of PANI onto the graphene-SPE a similar resistance was obtained (lilac curve, Rct = 624.5 Ω), indicating that the PANI is an excellent electric

conducting material which accelerated the electron transfer process. After covalent attachment of anti-α- amylase antibody, the Rct increased to 866.2 Ω (green curve), demonstrating that anti-alpha amylase was successfully immobilized on the PANI surface and blocked the electron exchange between the redox probe and the electrode. The Rct increased further when BSA was added to the SPE-graphene/PANI/Ab (red curve, Rct = 1454.7 Ω), due to the nonconductive nature of the protein.

3.6. α-amylase measurements in phosphate buffered saline (PBS), mouse and human plasma

PBS - Having determined the electrochemical properties of the functionalized sensor, the sensor was tested for its ability to measure amylase concentrations in a phosphate buffered solution that was used as a blood plasma mimic. Increasing amylase concentrations, from 1 to 500U/L, which covers the clinically relevant range of amylase levels in the human body, were applied to individual sensors. Both Nyquist plots (Figure 5C) and the resulting EIS calibration curve (Figure 5D) clearly demonstrate the effective response of the immunosensor to increasing amylase concentrations.

The diameter of the semicircle increased with increasing amylase concentrations demonstrating an increased resistance as a result of increased analyte concentration at the sensor surface. In general, the change in the semicircle diameter is a result of the change in the interfacial charge transfer resistance (Rct); that is, the resistance corresponding to the carrier transfer from the modified electrode to the ferricyanide in the solution. Thus, the observed diameter increase is explained as the adsorption of plasma onto anti-alpha amylase following an antigen–antibody reaction, where the adsorption of plasma effectively blocks the $[Fe(CN)6]^{3-/4-}$ leading to an increase of Rct. The Rct in the Nyquist plot increased linearly with the amylase concentrations. This is as expected because protein structures bound to the surface of an electrode typically act as barriers to electric transfer. The average slope of the Rct versus log [amylase, U/L] was 0.348 KΩ/[amylase, U/L] with an R^2 coefficient of determination of 0.93. The limit of detection (LOD) was 0.025U/L. This was as

expected as protein structures bound to the surface of an electrode typically act as barriers to electric transfer.

3.7. Mouse Plasma

In order to determine whether sensor function was effective when exposed to a complex biological fluid, mouse plasma containing known quantities of amylase were used. α-amylase concentrations were measured in un-spiked and plasma samples with purified human- α-amylase. The linear response ranged from 1 to 1000 U/L and the average slope was of 0.472 KΩ[amylase, U/L]. The EIS calibration curve of the immunosensor in response to increasing concentrations of amylase in mouse plasma showed no adverse effect on sensor performance in the presence of a more complex fluid compared to the PBS (Figure 6A).

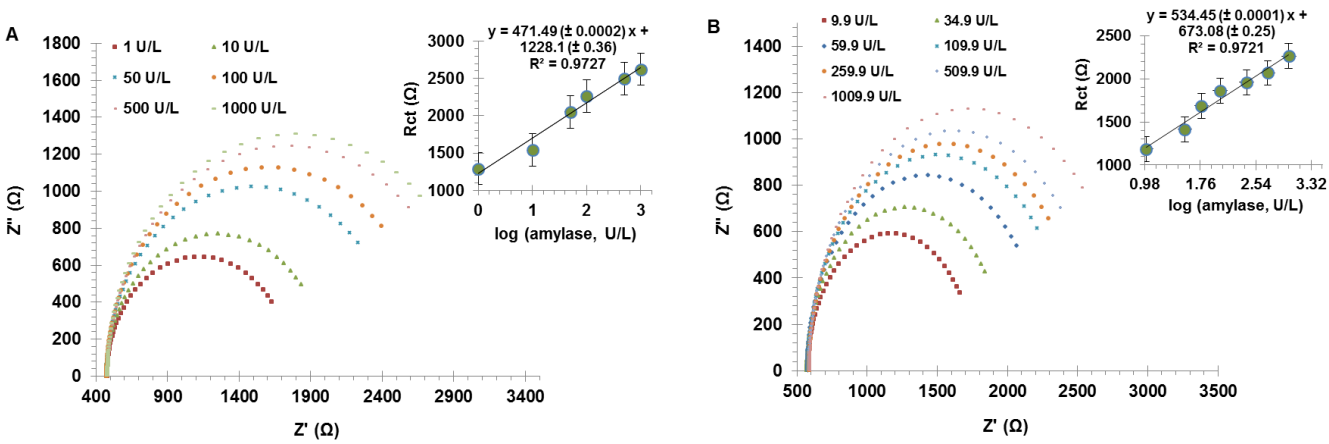

Figure 6. (A) Nyquist plots of BSA/anti-alpha amylase/PANI/graphene-SPE sensor, in 5.0mM $[Fe(CN)6]^{3-/4-}$ mouse plasma, previously incubated in increasing concentrations of amylase. Inset (A): corresponding calibration curve, plotting log(amylase) against Rct, with a standard deviation of 3.42%. (B) Nyquist plots corresponding to the calibration of the immunosensor in human plasma with amylase standards in U/L. Inset (B): corresponding calibration curve, plotting log(amylase) against Rct, with a standard deviation of 12.987%.

3.8. Human Plasma

To provide an initial demonstration of the potential clinical utility of the device, human plasma samples obtained from a patient suffering with clinical infection were analyzed. By spiking the human plasma with known concentrations of amylase we were able to determine the effectiveness and LOD of the sensor at physiologically relevant analyte concentrations.

Nyquist plots (Figure 6B) of EIS spectra show the dynamic range detectable when the sensor was exposed to various human plasma concentrations (9.9 – 1009.9 U/L).

In the development model used for this pilot study, the maximum interval to obtain a result was 300 seconds. In clinical practice, turnaround times (TAT) is a key indicator of laboratory performance (Chauhan et al., 2014). The current TAT for clinical assays in current practice is 45 min (Fei et al., 2015). Such studies, however, invariably omit the time taken for phlebotomy, transport of samples, and the interval from when samples are available to when they are picked up and interpreted by the attending physician. This is important when considering diseases whose mortality and morbidity increases with delayed diagnosis and clinical decision times (Debi et al., 2013). With optimisation and miniaturisation of the developmental model used in these studies, it is expected that the 300 second interval from loading a sample to obtaining a result will be substantially shortened. Moreover haemolysis, sample inactivation, and presence of contaminants interfering with colorimetric assays commonly lead to assay failure with current clinical assay systems. Since the system described in this study is label-free, and does not require either colorimetric change, it is reasonable to support the notion that the new technology will not be affected.

Finally, it is worth noting that the results indicate a three-log fold expansion in the lower limit of quantification when compared to current clinical assay systems (Bowling and Katayev 2010; Federal Drug Agency (FDA) 2015). This is of interest to forensic medicine where detection of amylase can lead to a DNA profile from saliva, semen or vaginal secretions (Casey and Price 2010).

4. Conclusion

The graphene-based label-free immune sensor we describe in this study represents a step change in the quantification of α-amylase. Quantitative, highly sensitive amylase sensing is achieved, with a wide limit of detection (0.025-1000 IU/L using spiked human blood plasma samples. Unlike current clinical assays, this technology is not based on enzymatic activity and/or colorimetric change, and would therefore not be affected by hemolysis, structural or functional inactivation of the amylase enzyme itself. The sensor design is compatible with miniaturization to a bedside diagnostic, avoiding the requirement for laboratory set-up, and the associated turnaround times, enabling the potential for a clinically compatible technology with a log fold expansion in the usable limits of quantification. The potential for a substantially more cost-effective, fully portable test that can be administered by the bedside, and the scalability for this diagnostic technology that can be achieved though standard semiconductor manufacturing techniques, would also expand the remit of such diagnostics beyond the secondary care sector, whilst avoiding the need for formal phlebotomy. Whilst retaining the potential for substantial cost-saving, and the possibility for expansion to multiplex and re-usable systems, the manufacture process is straightforward and easily applicable to any target molecule for which an antibody can be manufactured.

Acknowledgements

This work is funded by the European Social Fund (ESF) through the European Union's Convergence programme administered by the Welsh Government, Knowledge Economy Skills Scholarships (KESS), and St David's Medical Foundation. The authors would like to acknowledge Dr Dominic Fung for his help with SEM and Dr Greg Burwell for his help with Raman microscopy and BBI group for their contribution. The authors would like to acknowledge the Welsh National Research Network in Advanced Engineering and Materials (NRN). Research ethics council approval (REC 14/NE/1082) and local institutional R&D approval (T157) were obtained for the conduct of this study.

References

Ates, M., 2013. Mat Sci Eng C-Bio A 33, 1853-1859.

Azzopardi, E. A., Camilleri, L., Moseley, R; Thomas, D. W.; Ferguson, E. L., 2013. J Carbohyd Chem, 32, 438-449.

Azzopardi, E. Ferguson, E., Thomas, D., 2014. The Lancet 383.

Azzopardi, E. Lloyd, C.; Rodrigues Teixeira, S.; Conlan, R.; Whitaker, I., 2015. Surgery Manuscript No. 20150922 (Accepted for Publication).

Bhadra, S., Singha, N. K., and Khastgir, D., 2011. J Chem Eng J Mater Sci. 2, 1-11.

Bergkvist, M., Cady, N. C., 2011. Method Mol Cell Biol 751: 381-400.

Beitollah H., Goodarzian M., Khalilzadeh M. A., Karimi-Maleh H., Hassanzadeh M., Tajbakhsh M., 2012. J Mol Liq 173,137–143.

Bowling, J. L. and A. Katayev (2010). Lab Medicine 41(7): 398-402.

Casey, D. G. and J. Price (2010). Forensic science international 194(1): 67-71.

Chauhan, K. P.; Trivedi, A. P.; Patel, D.; Gami, B.; 2014. Haridas, N., Indian J Biochem 29, 505509. Chunmei Lv, Gao, X., Li, W., Xue, B., Qin, M., Burtnick, L. D., Zhou, H., Cao, Y., Robinson, R. C., Wang, W., 2014. Nat. Commun.

Dan Li; Mueller, M. B. G., Scott; Kaner, Richard B; Wallace, Gordon G, 2008. Nat. Nanotechnol. (3), 101.

Da-Wei, W.; Feng, L.; Jinping, Z.; Wencai, R.; Zhi-Gang, C.; Jun, T.; Zhong-Shuai, W.; Ian, G.; Gao Qing, L.; Hui-Ming, C., 2009. ACS nano, 3, 1745-1752.

Debi, U.; Kaur, R.; Prasad, K. K.; Sinha, S. K.; Sinha, A.; Singh, K., 2013. World J Gastroentero. 19, 9003.

Ding, J., Wang, M., Yan, X., Zhang, X., Ran, C., Chen, H., Yao, X., 2013. J Colloid Interf Sci. 395, 40-44.

Duncan, R., 2014. Toxicological Testing to Personalized Medicine.

Duncan, R., Gilbert, H., Carbajo, R., Vicent, M., 2008. Biomacromolecules. 9, 1146 - 1154.

Ebner, A., Wildling, L., Kamruzzahan, A.S., Rankl, C., Wruss, J., Hahn, C.D., Hölzl, M., Zhu, R., Kienberger, F., Blaas, D., Hinterdorfer, P., Gruber, H.J., 2007. Bioconjugate Chem. 18, 1176-1184.

Erhan, Z.; Imren, P.; Haluk, B.; Mustafa, E., 2013. Biosens Bioelectron. 42, 321-325.

Ensafi, A. A., Karimi-Maleh, H., 2010. J Electroanal Chem 640, 75–83.

Federal Drug Agency (FDA). (2015). http://www.accessdata.fda.gov/cdrh_docs/reviews/K040534.pdf.

Fei, Y.; Zeng, R.; Wang, W.; He, F.; Zhong, K.; Wang, Z., 2015. Biochem medica. 25, 213-221.

Fuhrmann R., Ros, A., 2010. Nanomedicine, 5, 657 - 666.

Gaspar, R.; Duncan. R., 2011. Mol. Pharmaceutics. 8, 2101 - 2141.

Hardwicke, J.; Ferguson, E. L.; Moseley, R.; Stephens, P.; Thomas, D. W.; Duncan, R., 2008. J Control Release130, 275-283.

Heli, H.; Sattarahmady, N.; Jabbari, A.; Moosavi-Movahedi, A. A.; Hakimelahi, G. H.; Tsai, F.Y., 2007. J Electroanal Chem. 610, 67-74.

Hyun Jung, L.; Sang Hyun, L.; Tomoyuki, Y.; Javier, R. A.; Fumio, M.; Kosuke, I.; Hitoshi, S.; Tomokazu, M., 2010. Talanta. 81, 657-663.

Li, J., Guo, S., Zhai, Y., Wang, E., 2009. Electrochem. Commun. 11, 1085.

Wang, Y.; Li, Z.; Wang, J.; Li, J.; Lin, Y., 2011. Trends Biotechnol. 29, 205-212

Jonathan, S. D., Nader, P. 2007. Electroanal. 19(12): 1239-1257.

Karimi-Maleh, H., Biparva, P., Hatami, M., 2013. Biosens Bioelectron 48, 270–275.

Karimi-Maleh, H., Tahernejad-Javazmi, F., Ensafi, A. A., Moradi R., Mallakpour, S., Beitollahi, H., 2014. Biosens Bioelectron 60, 1–7.

Lewis, W. F.; Paul, D. L.; Deyarina, G.; Timothy, A. R.; Gordon, W.; Lisa, A. J.; John, O. W.; Chris, J. W.; Conlan, R. S., 2009. Biology of the Cell. 101, 481-493.

Yueming, L., Longhua, T., Jinghong, L., 2009. Electrochem. Commun. 11, 846.

Kavitha, B., Kumar, K. S., Narsimlu, N., 2012. Indian J Pure Ap Phy. 51, 207-209.

Martin, P. 2011. Materials Today 14.

Moradi, R., Sebt, S. A., Karimi-Maleh, H., Sadeghi, R., Karimi, F., Baharie, A. Arabif, H., 2013. Phys. Chem. Chem. Phys.15, 5888.

Nafie, L. 2001. Handbook of Raman Spectroscopy, Practical Spectroscopy Series.

Neundlinger, I., Poturnayova, A., Karpisova, I., Rankl, C., Hinterdorfer, P., Snejdarkova, M., Hianik,T., Ebner, A., 2011. Biophys J. 101, 1781 - 1787.

Nguyen Xuan, V.; Miyuki, C.; Yoshiaki, U.; Kenzo, M.; Kazuhiko, M.; Eiichi, T.; Pham Hung, V.; Yuzuru, T., 2013. Biosens Bioelectron. 42, 592-597.

Pena-Pereira, F.; Duarte, R. M. B. O.; Duarte, A. C., 2012. Trends Anal Chem. 40, 90-105.

Pumera, M.; Ambrosi, A.; Bonanni, A.; Chang, E. L. K., 2010. Trends Anal Chem. Price, 2001. BMJ: British Medical Journal 322, 1285.

Qin, W.; Ru, L.; Bin, D.; Dan, W.; Yanyan, H.; Yanyan, C.; Yanfang, Z.; Xiaodong, X.; He, L.; Minghui, Y., 2011. Sensor Actuat B-Chem. 153.

Ruecha, N., Rodthongkum, N., Cate, D. M., Volckens, J., Chailapakul, O., Henry, C. S., 2015. Anal Chim Acta. 874, 40-48.

Seetharaman, K., Bertoft, E., 2012. Starch-Stärke 64, 765-769.

Song, L.; Xuefeng, G., 2012. NPG Asia Materials 4.

Srinives, S.; Sarkar, T.; Hernandez, R.; Mulchandani, A., 2015. Anal Chim Acta 874, 54-58.

Shahmiri, M. R., Bahari A., Karimi-Malehb, H., Hosseinzadeh, R., Mirnia, N., 2013. Sensor Actuator B 177, 70–77.

Teixeira S.; Conlan, R. S., Guy, O. J.; Sales, M. G. F., 2014. J Mat Chem B 2, 1852-1865.

Tothill, I. E. 2009. Seminars in Cell & Developmental Biology 20, 5562.

Toktam, N.; Brian, G. C.; Alexander, M. S., 2014. Arch Toxicol.

Wenjing, Y.; Yu, Z.; Yingru, L.; Chun, L.; Hailin, P.; Jin, Z.; Zhongfan, L.; Liming, D.; Gaoquan, S., 2013. Sci Rep 3, 22-48.

Whitcomb, D., M. Lowe 2007. Digest Dis Sci. 52, 1-17.

Yasufumi, T.; Andrew, I. S.; Pavel, N.; Yumi, M.; Hitoshi, S.; Yuri, E. K.; Tomokazu, M., 2010. J Am Chem Soc 132, 10118-10126.

Yi Cao, Balamurali, M. M., Sharma, D., Li, H., 2007. PNAS 104, 15677 - 15681.

Liu,Y., Deng, R., Wang, Z., Liu, H., 2012. J. Mater. Chem. 22, 13619-13624.

Zhang, Q.; Prabhu, A.; San, A.; Al-Sharab, J. F.; Levon, K., 2015. Biosens Bioelectron. 72, 100-106.

Zi-Long, W.; Rui, G.; Gao-Ren, L.; Han-Lun, L.; Zhao-Qing, L.; Fang-Ming, X.; Mingqiu, Z.; YeXiang, T., 2012. J Mat Chem. 22.

Zhixiang, Z.; Yongling, D.; Qingliang, F.; Zaihua, W.; Chunming, W., 2012. J Mol Catal A-Chem. 353-354.

Highlights

- Sensitive α-amylase immunosensor platform, produced via *in situ* electropolymerization of aniline onto a screen-printed graphene support (SPE).
- Fully quantitative, highly sensitive alpha-amylase biosensing.
- Specific attachment of anti alpha-amylase to modified graphene devices.
- The device has a remarkably wide limit of quantification (0.025-1000 IU/L) compared to alpha-amylase assays in current clinical use.